

# Determination of the In-Plane Exciton Radius in 2D CdSe Nanoplatelets via Magneto-optical Spectroscopy

Alexandra Brumberg,<sup>†</sup> Samantha M. Harvey,<sup>†,‡</sup> John P. Philbin,<sup>§</sup> Benjamin T. Diroll,<sup>||</sup> Byeongdu Lee,<sup>⊥</sup> Scott A. Crooker,<sup>#</sup> Michael R. Wasielewski,<sup>†,‡</sup> Eran Rabani,<sup>§,¶,△</sup> and Richard D. Schaller<sup>\*,†,||</sup>

<sup>†</sup>Department of Chemistry and <sup>‡</sup>Institute for Sustainability and Energy at Northwestern, Northwestern University, Evanston, Illinois 60208, United States

<sup>§</sup>Department of Chemistry, University of California, Berkeley, California 94720, United States

<sup>||</sup>Center for Nanoscale Materials and <sup>⊥</sup>Advanced Photon Source, Argonne National Laboratory, Lemont, Illinois 60439, United States

<sup>#</sup>National High Magnetic Field Laboratory, Los Alamos National Laboratory, Los Alamos, New Mexico 87545, United States

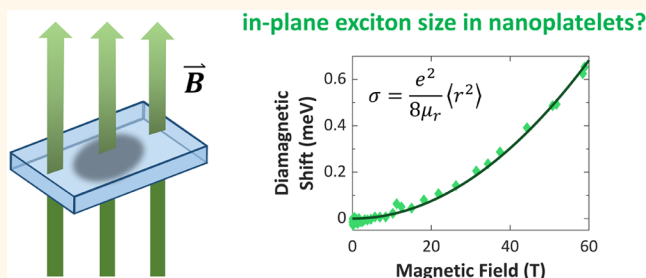
<sup>¶</sup>The Sackler Center for Computational Molecular and Materials Science, Tel Aviv University, Tel Aviv 69978, Israel

<sup>△</sup>Materials Science Division, Lawrence Berkeley National Laboratory, Berkeley, California 94720, United States

## Supporting Information

**ABSTRACT:** Colloidal, two-dimensional semiconductor nanoplatelets (NPLs) exhibit quantum confinement in only one dimension, which results in an electronic structure that is significantly altered compared to that of other quantum-confined nanomaterials. Whereas it is often assumed that the lack of quantum confinement in the lateral plane yields a spatially extended exciton, reduced dielectric screening potentially challenges this picture. Here, we implement absorption spectroscopy in pulsed magnetic fields up to 60 T for three different CdSe NPL thicknesses and lateral areas. Based on diamagnetic shifts, we find that the exciton lateral extent is comparable to NPL thickness, indicating that the quantum confinement and reduced screening concomitant with few-monolayer thickness strongly reduces the exciton lateral extent. Atomistic electronic structure calculations of the exciton size for varying lengths, widths, and thicknesses support the substantially smaller in-plane exciton extent.

**KEYWORDS:** nanoplatelets, exciton size, quantum confinement, diamagnetic shift, electronic structure



Semiconductor nanoplatelets (NPLs) present thicknesses that are smaller than the bulk excitonic Bohr radius, and yet they are quasi-infinite in lateral extent. Given the strong, thickness-defined quantum confinement, NPLs constitute colloidal analogues of epitaxially grown quantum wells. In the case of zinc blende CdSe, NPLs with three to eight monolayers (MLs) of roughly 0.3 nm each can be synthesized with negligible ensemble thickness dispersity<sup>1–4</sup> as well as lengths and widths of tens of nanometers, as detailed in Figure 1.<sup>1,5–7</sup> Given the 5.4 nm bulk CdSe Bohr radius, this scenario might suggest pancake-like, nearly two-dimensional excitons with a large value for the in-plane exciton radius,  $r_{\text{plane}} \approx r_l \approx r_w$  (see Figure 1a). On the other hand, interplay between confinement energy and electron–hole Coulomb attraction may yield a small and relatively spherical exciton with  $r_h \approx r_l \approx$

$r_w$ . Given the synthetic control over thickness and (to a lesser degree) lateral extent of the two-dimensional morphology,<sup>1,8–13</sup> CdSe NPLs present an ideal material for examination of this fundamental question.

Since the first detailed report of CdSe NPLs,<sup>1</sup> the topic of excitons in CdSe NPLs has been treated theoretically,<sup>14–17</sup> but with only one explicit calculation of exciton size.<sup>20</sup> As in ref 20, estimates regarding exciton size can be developed based on the exciton binding energy,<sup>18</sup> but discrepancies in reports of this energy exist, with experimental and theoretical papers

Received: March 13, 2019

Accepted: June 17, 2019

Published: June 17, 2019

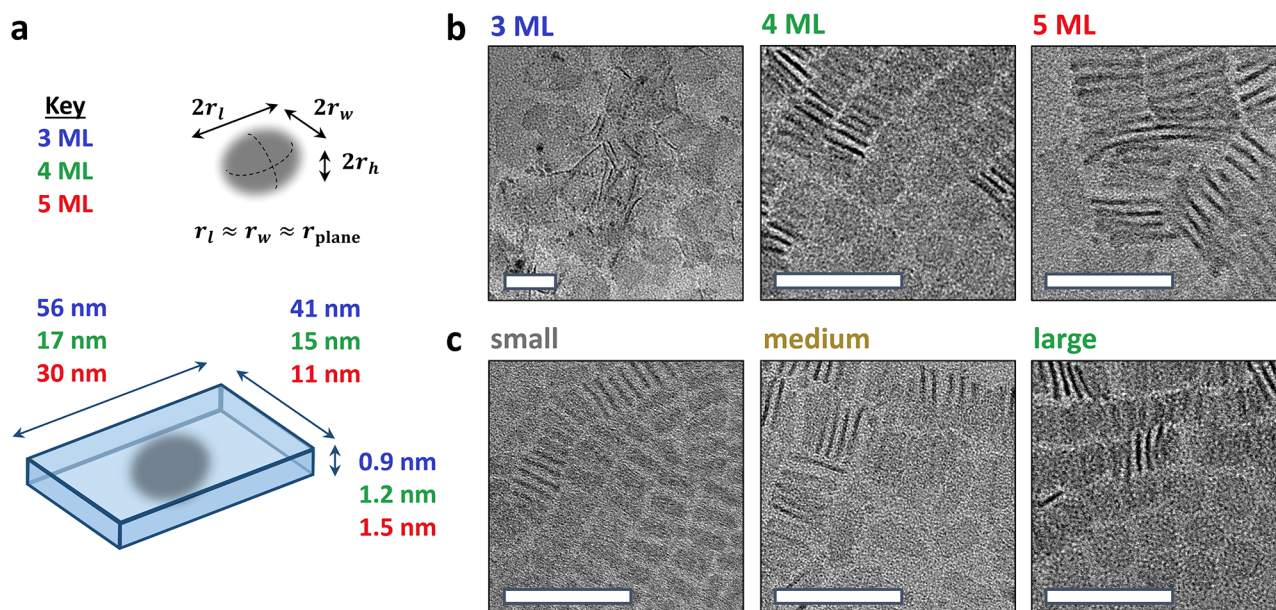


**Figure 1.** (a) Diagram depicting representative dimensions of a CdSe NPL. The shaded gray region represents the exciton, which has dimensions  $2r_l \times 2r_w \times 2r_h$ . (b,c) Transmission electron microscopy images of (b) 3, 4, and 5 ML CdSe NPLs and (c) small, medium, and large lateral area 4 ML CdSe NPLs. Scale bars are 50 nm.

conveying values ranging from about 100 meV to greater than 400 meV.<sup>14,15,19,20</sup> Derived values also depend upon whether the structures are treated using 3D or 2D Coulomb potentials. Whereas it is apparent that the change in dimensionality from three-dimensional bulk material to quasi-two-dimensional NPLs increases the exciton binding energy through reduced dielectric screening, as is the case with monolayer transition metal dichalcogenides,<sup>21,22</sup> it is not clear to what degree this alters the lateral exciton extent.

Treatments of excitons in conventional quantum wells offer a starting point for determining the lateral size of the exciton in NPLs. Calculations of exciton binding energies in GaAs and GaAs/Ga<sub>1-x</sub>Al<sub>x</sub>As quantum wells yield values on the order of tens of meV.<sup>23,24</sup> Given such small binding energies, excitons in quantum wells can be expected to have a large in-plane lateral extent. On the other hand, work by Miller notes that the exciton in a quantum well may be compressed not just vertically, due to potential changes at the well faces, but also laterally, so as to minimize orbital kinetic energy.<sup>25,26</sup> Results from quantum wells cannot necessarily be extrapolated to NPLs, given the finite lateral sizes of NPLs and their interactions with lower dielectric constant ligands, in comparison to semiconductor templating substrates.

Studies on two-dimensional transition metal dichalcogenides provide an additional, relevant comparison. Work probing monolayer WS<sub>2</sub> and WSe<sub>2</sub> suggests that the exciton lateral extent is between 1 and 2 nm,<sup>27–30</sup> consistent with large binding energies on the order of 200–500 meV.<sup>21,22,31</sup> These results suggest that the exciton in colloidal, quasi-two-dimensional NPLs may also be small; however, the potentially smaller binding energy in CdSe NPLs (which arises due to their smaller electron and hole mass and multilayer thickness) could engender a more spatially extended exciton.

Exciton size can be accessed *via* magneto-optical measurements. In a magnetic field, the energy of the exciton is modified and can be expressed as

$$E_{\pm}(B) = E_0 \pm \frac{1}{2}g_{\text{ex}}\mu_B B + \sigma B^2 + \dots \quad (1)$$

where  $E_0$  is the unperturbed exciton energy,  $g_{\text{ex}}$  is the excitonic g-factor,  $\mu_B$  is the Bohr magneton, and  $\sigma$  is the diamagnetic shift coefficient. The application of a magnetic field induces a linear Zeeman splitting that lifts the degeneracy of the exciton angular momentum states and introduces a diamagnetic shift term, which grows quadratically with the field. In magnetic fields where the cyclotron energy ( $\hbar eB/\mu_r$ ) is significantly smaller than the exciton binding energy, the diamagnetic shift coefficient is equivalent to

$$\sigma = \frac{e^2}{8\mu_{r,\text{plane}}} \langle r^2 \rangle \quad (2)$$

where  $e$  is the elementary charge,  $\mu_{r,\text{plane}}$  is the in-plane exciton reduced mass, and  $r$  is a radial coordinate in the direction perpendicular to the field.<sup>32,33</sup> Thus,  $\langle r^2 \rangle$  is the expectation value of  $x^2 + y^2$  with respect to the exciton wave function. When NPLs are oriented perpendicular to the direction of the applied magnetic field,  $\langle r^2 \rangle$  provides a measure of the in-plane exciton radius. Note that the root-mean-square exciton radius,  $r_{\text{rms}} = \sqrt{\langle r^2 \rangle}$ , is not the same as the often-used Bohr radius,  $a_B$ ; in bulk semiconductors,  $r_{\text{rms}} = \sqrt{2}a_B$ . With diamagnetic shift coefficients on the order of  $1 \mu\text{eV}/\text{T}^2$ , even 60 T magnetic fields only provide energy shifts of a few meV. As indicated in Table 1, the cyclotron energy (tens of meV) at these high fields remains an order of magnitude less than the (100 meV or greater) exciton binding energy in CdSe NPLs, such that the in-plane exciton radius can be calculated *via* a diamagnetic shift. This approach has previously been implemented to experimentally probe exciton radii in two-dimensional materials such as monolayer transition metal dichalcogenides and quantum wells.<sup>27–29,32,34–36</sup>

Determination of the in-plane exciton radius,  $r_{\text{plane}}$ , requires orientation of NPLs such that their lateral areas are perpendicular to the direction of the applied magnetic field.

**Table 1. Reduced Masses, Cyclotron Energies, and Binding Energies of the Heavy-Hole Excitons in 3, 4, and 5 ML CdSe NPLs (Reduced Masses Are from Ref 15)**

sample	reduced mass ( $m_0$ )	cyclotron energy at 60 T (meV)	binding energy (meV)
3 ML	0.21	33	~210
4 ML	0.17	41	~190
5 ML	0.14	49	~170

Orientation of CdSe NPLs has previously been attempted by incorporating NPLs into polymer films with subsequent stretching<sup>37,38</sup> or by manipulating solvent interfaces upon NPL monolayer deposition.<sup>39–41</sup> For optical measurements in magnetic fields, the former option presents advantages with regard to the optical density required for absorption measurements.

In this work, CdSe NPLs were first oriented by biaxially stretching polymer films and probed using small-angle X-ray scattering (SAXS), which determined that sufficient in-plane orientation was successfully achieved. Optical absorption spectra of both unstretched and stretched films were then measured *versus* magnetic field strength at low temperature to calculate diamagnetic shift coefficients, covering three different thicknesses and lateral areas. The observed diamagnetic shifts are small and support a picture of tightly bound excitons with small lateral extent. Atomistic calculations, conducted by using a semiempirical pseudopotential method<sup>42,43</sup> and solving of the Bethe–Salpeter equation<sup>44</sup> that accounts for electron–hole interactions, are consistent with the experimental findings.

## RESULTS AND DISCUSSION

CdSe NPLs of 3, 4, and 5 ML thickness as well as small, medium, and large lateral areas of 4 ML thickness were synthesized according to previous reports.<sup>6,9,45</sup> As shown in Figure 1, the NPLs studied here feature thicknesses of 0.9, 1.2, and 1.5 nm for 3, 4, and 5 ML NPLs, respectively. Both 4 and 5 ML NPLs typically have widths and lengths around 10–30 nm, whereas currently accessible 3 ML NPLs yield larger lateral size greater than 40 nm across in both directions.<sup>6</sup> In these experiments, NPLs were dispersed in a solution of chloroform and poly(butyl methacrylate-*co*-isobutyl methacrylate) and drop-cast to form low-scatter films that were then biaxially stretched (see Methods).

To discern whether stretching achieved in-plane orientation of NPLs, SAXS data were acquired in both transmission and reflection geometries. Figure 2 shows SAXS data for polymer films containing 5 ML NPLs, before and after applying biaxial strain (data for 3 and 4 ML NPLs appear as Supporting Information Figures S2 and S3). Prior to stretching, the transmission pattern (Figure 2a) is isotropic, indicating no net NPL orientation in the plane of the film. Anisotropy of the reflection mode pattern (stronger scattering in the horizontal direction, as shown in Figure 2b) additionally suggests that NPLs preferentially orient perpendicular to the plane of the film in stacks, as has been previously observed.<sup>38,46,47</sup> After being stretched, the transmission and reflection scattering signals (Figures 2c,d) are present at the same  $q$  value as before, indicating that stacks of NPLs remain with the same spacing. However, the lack of transmission scattering intensity at most detection azimuthal angles in Figure 2c suggests that many of the stacks with perpendicularly oriented NPLs have broken apart or rotated from a perpendicular orientation to one in

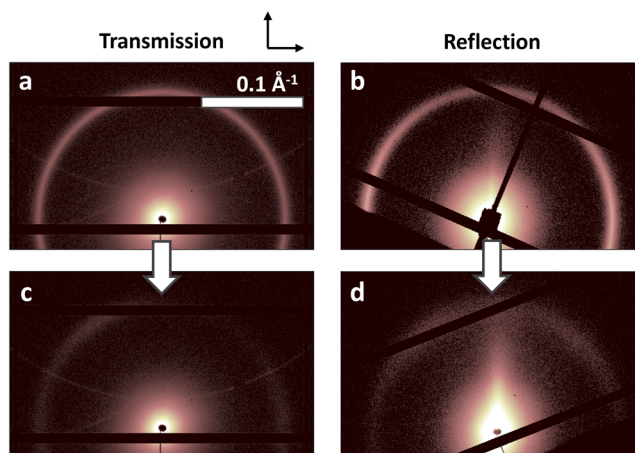


**Figure 2. Transmission (left column) and reflection (right column) SAXS images of films containing 5 ML CdSe NPLs in polymer (a,b) before and (c,d) after stretching. Stretching axes are roughly identified by the two black arrows. Intensities are logarithmic and are only consistent between the transmission patterns.**

which the stacks lay within the plane of the film. This rotation is corroborated by the reversal of scattering intensity from being primarily in the horizontal direction (Figure 2b) to being primarily in the vertical direction (Figure 2d).

It should be noted that, as shown in Figure 2, the scattering intensity after stretching decreases significantly. In part, this is due to a reduction in stretched film thickness (by up to a factor of 4). However, there is the additional consideration that stretching breaks up some of the NPL stacks, as highlighted by the significant reduction of scattering intensity in Figure 2c,d and as has been reported previously.<sup>38</sup> The broad vertical streak in Figure 2d suggests that the majority of NPLs are not arranged within stacks (which would appear within the ring at higher  $q$ ) and are instead separated. Unfortunately, for those NPLs that are not arranged in stacks, there is no quantitative way to determine their orientation relative to the plane of the film. However, literature on polymer composites suggests that single NPLs likely align parallel to the flow direction,<sup>48</sup> although the degree to which this would occur may be subject to the interaction between the NPLs and the polymer matrix.<sup>49</sup>

Optical spectroscopy in pulsed magnetic fields up to 60 T was performed on CdSe NPLs in stretched polymer films at 4 K. Circularly polarized light, produced by a polarizer, facilitates probing of the different heavy-hole exciton angular momentum states, as optical selection rules dictate that  $\Delta m = +1$  for left circularly polarized light ( $\sigma^-$ ) and  $\Delta m = -1$  for right circularly polarized light ( $\sigma^+$ ). Pulsing the magnetic field in both the positive (to +60 T) or negative (to –60 T) directions permits access to each polarization state with a fixed polarizer, as these are equivalent by time-reversal symmetry.

Figure 3a shows transmission spectra at 4 K of 3, 4, and 5 ML NPLs at 0 T. (Absorption spectra at room temperature for all samples appear in Supporting Information Figure S1.) Upon application of a magnetic field, the band-edge heavy-hole exciton peak shifts, as shown in Figure 3b, and is accompanied by a slight change in the line shape. To track the shift of the heavy-hole exciton in the magnetic field, a linear baseline was subtracted from the transmission spectrum and the peak was fit to a Gaussian function (see the Supporting Information for further description of the analysis). The resulting peak

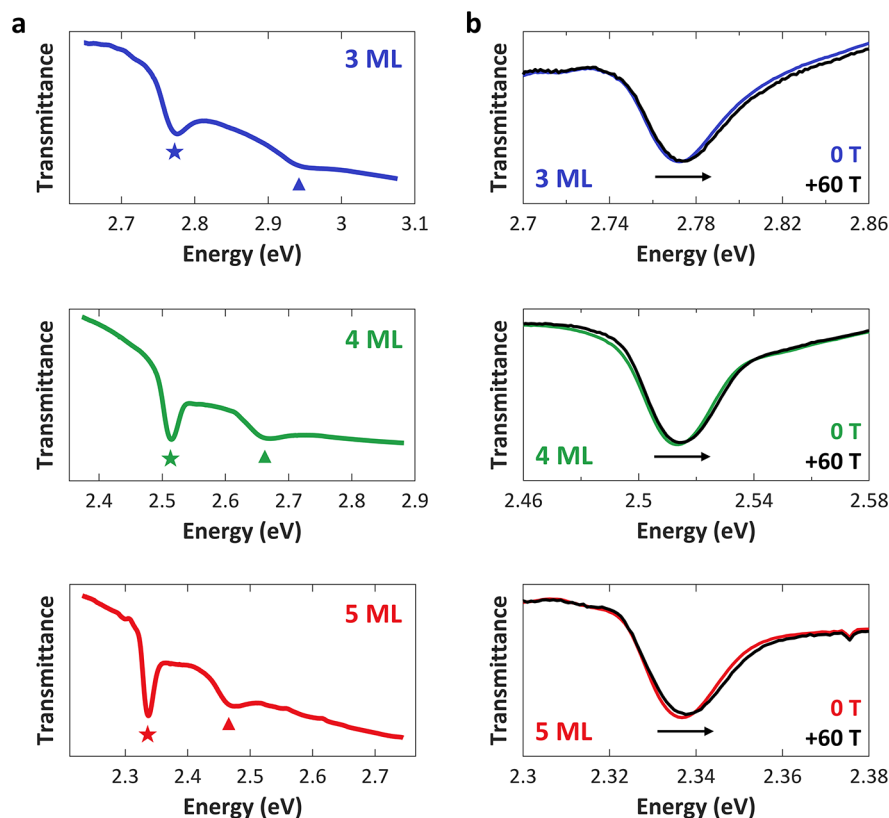


**Figure 3.** (a) Transmission spectra of 3, 4, and 5 ML CdSe NPLs at 0 T (no applied magnetic field) and 4 K. Stars and triangles indicate the heavy-hole and light-hole/split-off exciton transitions, respectively. (b) Baseline-subtracted spectra of 3, 4, and 5 ML CdSe NPLs at 4 K with an applied magnetic field of 0 and 60 T, showing the shift in heavy-hole exciton energy with the magnetic field (as indicated by the arrow in each panel).

positions were then used as inputs for fitting to eq 1 to obtain the diamagnetic shift coefficient,  $\sigma$ .

Figure 4 shows the shifts in exciton energy as a function of magnetic field for CdSe NPLs in stretched polymer films. The solid lines depict fits of the data to eq 1, from which the values of the excitonic  $g$ -factors (see Supporting Information Table S3) and the diamagnetic shift coefficients are obtained. Notably, by plotting the average exciton energy,  $(E_+ + E_-)/2 = \sigma B^2$ , as in Figure 5b for 5 ML NPLs and Supporting Information Figure S6 for other NPLs, a diamagnetic shift is observed. This shift is clearly quadratic through the full 60 T range, consistent with our estimate that the magnetic fields accessed act as weak perturbations on the tightly bound CdSe NPL excitons. Thus, eq 2 is appropriate for conversion of the observed diamagnetic shift coefficients to the root-mean-square in-plane exciton radius.

The in-plane exciton radius depends not only on  $\sigma$ , the measured diamagnetic shift coefficient, but also  $\mu_{r,\text{plane}}$ , the in-plane reduced mass of the heavy-hole exciton, which we do not experimentally access. Reports of  $\mu_{r,\text{plane}}$  vary between  $0.14m_0$  and  $0.21m_0$  (where  $m_0$  is the free electron mass), depending on the literature source and NPL thickness.<sup>1,15,50</sup> The small diamagnetic shifts of 0.15–0.21  $\mu\text{eV}/\text{T}^2$  reported in Figure 4 thus suggest in-plane exciton radii in the range of 1.1–1.4 nm for all probed samples. This is significantly smaller than the bulk exciton Bohr radius of 5.4 nm for bulk CdSe and consistent with large exciton binding energies.

It is important to emphasize that the magnitude of the diamagnetic shift depends on NPL net orientation. When NPLs lie flat in the plane of the polymer film, perpendicular to

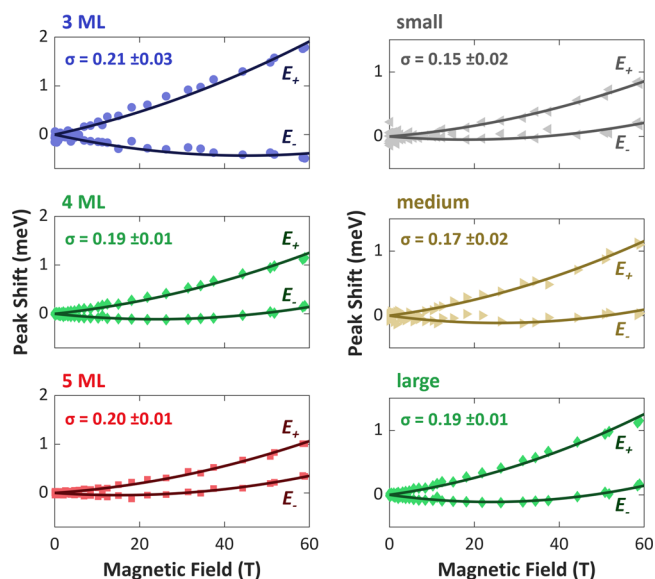


**Figure 4.** Heavy-hole exciton peak shifts for 3, 4, or 5 ML thickness NPLs and for 4 ML NPLs of small, medium, or large lateral area. The vertical scale is consistent between panels in the same column. Diamagnetic shift coefficients for each sample are indicated in units of  $\mu\text{eV}/\text{T}^2$ .

the direction of the applied magnetic field, a greater diamagnetic shift is expected than when NPLs lie parallel to the direction of the field. Notably, as the exciton lateral extent approaches its vertical extent (approaching a spherical

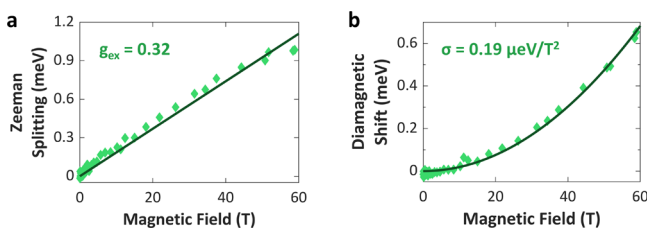


**Figure 5.** (a) Zeeman splitting for the large 4 ML NPLs, obtained by taking the difference between the excitonic energy as a function of the field. The relation  $g_{\text{ex}}\mu_B B = E_+ - E_-$  yields an excitonic  $g$ -factor of 0.32. (b) Diamagnetic shift, isolated by taking the average excitonic energy of the two states  $E_{\text{avg}} = (E_+ + E_-)/2$ , for the 4 ML NPLs. The shift can be fit to  $\sigma B^2$  to obtain a diamagnetic shift coefficient of  $\sigma = 0.19 \mu\text{eV}/\text{T}^2$ . Zeeman splittings and diamagnetic shifts for all other samples appear as Supporting Information Figures S5 and S6, respectively.

exciton), net orientation effects diminish. Conversely, if the exciton lateral extent approaches large values such as the bulk Bohr radius (5.4 nm), the observed diamagnetic shift increases quadratically. For example, for an in-plane exciton radius of 2.4 nm, twice as large as the  $\sim 1.2$  nm radius observed here, a  $0.8 \mu\text{eV}/\text{T}^2$  diamagnetic shift coefficient would result, which is 4 times greater than that observed experimentally. Such a difference would be discernible in these measurements. As a result of this behavior, the possibility that the in-plane exciton radius reported in this work of  $\sim 1.2$  nm is a result of poor orientation, rather than an actual small exciton size, is small.

To further probe how NPL dimensions impact exciton size and whether theoretical pictures of NPLs reflect the experiment, we performed atomistic electronic structure calculations for a series of 3, 4, and 5 ML CdSe NPLs (see Supporting Information for details). Calculations were performed on Cd-terminated NPLs that implement the bulk zinc blende CdSe lattice constant of 0.6058 nm. Ligand potentials used to passivate the NPL were taken from ref 43. The filter-diagonalization technique<sup>51,52</sup> was used to obtain the electron and hole states that were then used to solve the Bethe–Salpeter equation.<sup>44</sup>  $\langle r^2 \rangle$  was calculated using the resulting excitonic (*i.e.*, correlated electron–hole) wave function. The exciton energy, binding energy, and  $\langle r^2 \rangle$  were converged with respect to the number of electron and hole states used when solving the Bethe–Salpeter equation.

Each calculated series spans a range of NPL lateral sizes, beginning with lateral dimensions smaller than the bulk exciton Bohr radius (4 nm  $\times$  4 nm) and ending with lateral dimensions approaching twice the size of the bulk exciton Bohr radius (8 nm  $\times$  8 nm). The calculated in-plane exciton radii (shown in Figure 6) are of similar magnitude to the experimentally determined in-plane exciton radii, in the range of 1.0–1.5 nm depending only weakly on the NPL thickness and lateral area. The increase of the in-plane exciton radius with increasing NPL dimensions (both lateral area and thickness) can be justified on account of the reduction in Coulombic attraction between the electron and hole when the volume of the NPL is increased. Notably, although dielectric screening affects the overall lateral extent of the exciton, the exciton spatial extent remains small (in the range of 1.2–2.0 nm) even when a larger, less warranted dielectric constant is chosen (see Table S5 and the discussion in the Supporting Information).

The measured and calculated small, in-plane exciton radii found here are consistent with reports for other 2D structures,

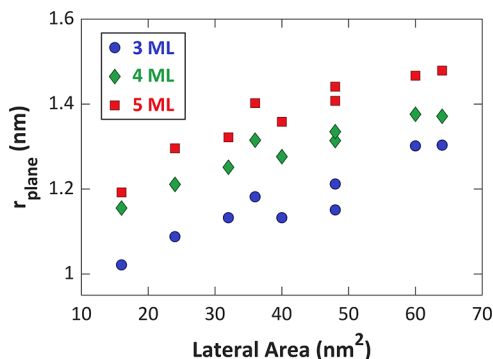


**Figure 6.** Atomistic electronic structure calculations of  $r_{\text{plane}}$  for 3, 4, and 5 ML CdSe NPLs of varying lateral sizes.

such as transition metal dichalcogenides. An often-invoked explanation for the small exciton size is based on reduced screening, where the electron and hole interact through the surrounding lower dielectric environment, leading to localization of the electron–hole pair, but are also consistent with pictures of minimized orbital kinetic energy. Future investigations will focus on tuning the surrounding dielectric screening so as to manipulate exciton spatial extent and probe the degree to which NPL dielectric properties determine exciton size owing to finite NPL thickness.

## CONCLUSION

In conclusion, we have prepared films of oriented CdSe NPLs by embedding NPLs in stretched polymer films. Absorption measurements in pulsed magnetic fields show that the heavy-hole exciton energy shifts with the applied field in a way that can be characterized *via* the diamagnetic shift coefficient. Diamagnetic shifts of three different thickness and three different lateral area NPLs reveal that the in-plane exciton radius of CdSe NPLs is in each case small, despite the lateral dimensions exceeding those of the conventional bulk CdSe Bohr radius. Atomistic modeling using realistic, discrete NPL structures arrives at similar  $r_{\text{plane}}$  values and supports the hypothesis that the NPL exciton is a small and relatively compact spheroid.

## METHODS

**Synthesis of CdSe Nanoplatelets.** CdSe NPLs were synthesized according to previously published procedures with slight modifications.<sup>6,9</sup>

**3 ML NPLs:** Cadmium acetate (240 mg), oleic acid (150 mL), and octadecene (15 mL) were added to a three-neck flask and degassed for 1 h at 80 °C. The solution was then heated to 180 °C under nitrogen, at which point selenium powder in trioctylphosphine (150  $\mu\text{L}$ , 1 M) was rapidly injected. After 5 min, the reaction was stopped and the NPLs were washed twice with isopropyl alcohol and then redispersed in 1-methylcyclohexane.

**4 ML NPLs:** Cadmium myristate (170 mg), selenium powder (12 mg), and octadecene (14 mL) were added to a three-neck flask and degassed for 1 h under stirring. The solution was then heated under nitrogen; when the temperature reached 190 °C, cadmium acetate (40 mg) was added. To achieve small plates, the solution was heated to 225 °C and then cooled. To achieve medium or large plates, the solution was heated to and then held at 240 °C for 1 min (medium plates) or 5 min (large plates) and then cooled. When the temperature reached 70 °C during cooling, oleic acid (2 mL) and hexane (15 mL) were added. The solution was then centrifuged, and the resulting pellet was dissolved in 1-methylcyclohexane and filtered through a 0.2  $\mu\text{m}$  PTFE syringe filter.

**5 ML NPLs:** Cadmium myristate (170 mg) and octadecene (14 mL) were added to a three-neck flask and then degassed for 30 min. The solution was then heated to 250 °C. At 250 °C, selenium powder (12 mg) sonicated in octadecene (1 mL) was rapidly injected. After 60 s, cadmium acetate (90 mg) was added. The solution was held at 250 °C for 10 min and then cooled. When the temperature reached 70 °C, oleic acid (2 mL) and hexane (15 mL) were added. The solution was then centrifuged and the resulting pellet was dissolved in 1-methylcyclohexane and filtered through a 0.2  $\mu\text{m}$  PTFE syringe filter.

**Preparation of Polymer Films.** A 5 wt % solution of poly(butyl methacrylate-*co*-isobutyl methacrylate) in chloroform was prepared by dissolving the polymer (460 mg) in chloroform (10 mL). The desired amount of CdSe NPLs was dried in a small vial and redispersed in 400–450  $\mu\text{L}$  of the polymer solution. The solution was mixed using a Vortex mixer to ensure full dispersion of the NPLs. The entire 400–450  $\mu\text{L}$  of solution was then deposited on a 22 mm  $\times$  22 mm glass coverslip and allowed to dry.

Before being stretched, the polymer films were removed from the glass substrates using a razor blade. Binder clips were attached to two opposing ends of the films on top of 2 cm  $\times$  5 mm glass pieces wrapped in Teflon tape to evenly distribute the stretching force along the sides of the film. The film was then placed in a hot water bath heated to above the glass transition temperature of the polymer (35 °C) before stretching along the first axis. After being allowed to cool, an additional set of binder clips were added to the remaining two sides. The film was once again placed in the bath, and the film was stretched along the second axis while maintaining force along the first axis. The film was allowed to cool before the clips were removed. The films were typically stretched to 200% along the first axis and to just less than 200% along the second axis.

**Small-Angle X-ray Scattering.** Small-angle X-ray scattering was conducted using Beamline 12 ID-B at the Argonne National Laboratory Advanced Photon Source using 13.3 keV X-rays. The scattered radiation was detected using a Pilatus detector approximately 2 m away from the sample. A silver behenate sample was used as a standard for  $q$  calibration.

**Absorption Measurements in Magnetic Fields.** Absorption measurements in high magnetic fields were acquired at 4 K using a 65 T pulsed magnet located at the National High Magnetic Field Laboratory in Los Alamos, NM. An optical fiber was used to deliver white light from a xenon lamp through a thin-film circular polarizer and the sample. The transmitted light was reflected back into a collection fiber and into a 300 mm spectrometer with a CCD detector, which was synchronized to the magnetic field pulse.

## ASSOCIATED CONTENT

### Supporting Information

The Supporting Information is available free of charge on the ACS Publications website at DOI: [10.1021/acsnano.9b02008](https://doi.org/10.1021/acsnano.9b02008).

Calculations to support the claim of a low magnetic field regime, absorption spectra of samples at room temperature, SAXS data for 3 and 4 ML NPLs, description of data processing techniques, excitonic  $g$ -factors, diamagnetic shifts, and computational details (PDF)

## AUTHOR INFORMATION

### Corresponding Author

\*E-mail: [schaller@anl.gov](mailto:schaller@anl.gov) or [schaller@northwestern.edu](mailto:schaller@northwestern.edu).

### ORCID

Alexandra Brumberg: 0000-0003-2512-4686

John P. Philbin: 0000-0002-8779-0708

Benjamin T. Diroll: 0000-0003-3488-0213

Scott A. Crooker: 0000-0001-7553-4718

Michael R. Wasielewski: 0000-0003-2920-5440

Richard D. Schaller: 0000-0001-9696-8830

## Author Contributions

B.T.D. synthesized the nanoparticles and collected transmission electron microscopy images. A.B., S.M.H., and B.T.D. prepared polymer films. A.B., S.M.H., and B.L. collected small-angle X-ray scattering data. A.B., S.M.H., R.D.S., and S.A.C. conducted the magneto-optical measurements. A.B. analyzed the experimental data under the guidance of R.D.S. and S.A.C. J.P.P. and E.R. developed the atomistic simulation approach and codes, and J.P.P. performed the atomistic calculations. All authors contributed to the writing of this manuscript.

## Notes

The authors declare no competing financial interest.

## ACKNOWLEDGMENTS

This material is based upon work supported by the National Science Foundation under Grant Nos. DMREF-1629383 and DMREF-1629361, as well as by the National Science Foundation Graduate Research Fellowship Program under Grant No. DGE-1324585 (A.B., S.M.H.). A portion of this work was performed at the National High Magnetic Field Laboratory, which is supported by National Science Foundation Cooperative Agreement Nos. DMR-1157490 and 1644779, the U.S. Department of Energy, and the State of Florida. This work was supported by the U.S. Department of Energy, Office of Science, Office of Basic Energy Sciences under Award DE-FG02-99ER14999. This research used resources of the Advanced Photon Source (Argonne National Laboratory) and the National Energy Research Scientific Computing Center (NERSC), which are U.S. Department of Energy (DOE) Office of Science User Facilities operated under Contract Nos. DE-AC02-06CH11357 and DE-AC02-05CH11231, respectively. Use of the Center for Nanoscale Materials, an Office of Science user facility, was supported by the U.S. Department of Energy, Office of Science, Office of Basic Energy Sciences, under Contract No. DE-AC02-06CH11357.

## REFERENCES

- (1) Ithurria, S.; Tessier, M. D.; Mahler, B.; Lobo, R. P. S. M.; Dubertret, B.; Efros, A. L. Colloidal Nanoplatelets with Two-Dimensional Electronic Structure. *Nat. Mater.* **2011**, *10*, 936–941.
- (2) Tessier, M. D.; Javaux, C.; Maksimovic, I.; Lorient, V.; Dubertret, B. Spectroscopy of Single CdSe Nanoplatelets. *ACS Nano* **2012**, *6*, 6751–6758.
- (3) Cho, W.; Kim, S.; Coropceanu, I.; Srivastava, V.; Diroll, B. T.; Hazarika, A.; Fedin, I.; Galli, G.; Schaller, R. D.; Talapin, D. V. Direct Synthesis of Six-Monolayer (1.9 nm) Thick Zinc-Blende CdSe Nanoplatelets Emitting at 585 nm. *Chem. Mater.* **2018**, *30*, 6957–6960.
- (4) Christodoulou, S.; Climente, J. I.; Planelles, J.; Brescia, R.; Prato, M.; Martín-García, B.; Khan, A. H.; Moreels, I. Chloride-Induced Thickness Control in CdSe Nanoplatelets. *Nano Lett.* **2018**, *18*, 6248–6254.
- (5) Bertrand, G. H. V.; Polovitsyn, A.; Christodoulou, S.; Khan, A. H.; Moreels, I. Shape Control of Zincblende CdSe Nanoplatelets. *Chem. Commun.* **2016**, *52*, 11975–11978.
- (6) She, C.; Fedin, I.; Dolzhenkov, D. S.; Dahlberg, P. D.; Engel, G. S.; Schaller, R. D.; Talapin, D. V. Red, Yellow, Green, and Blue Amplified Spontaneous Emission and Lasing Using Colloidal CdSe Nanoplatelets. *ACS Nano* **2015**, *9*, 9475–9485.
- (7) Bose, S.; Song, Z.; Fan, W. J.; Zhang, D. H. Effect of Lateral Size and Thickness on the Electronic Structure and Optical Properties of Quasi Two-Dimensional CdSe and CdS Nanoplatelets. *J. Appl. Phys.* **2016**, *119*, 143107.

- (8) Chikan, V.; Kelley, D. F. Synthesis of Highly Luminescent GaSe Nanoparticles. *Nano Lett.* **2002**, *2*, 141–145.
- (9) Ithurria, S.; Dubertret, B. Quasi 2D Colloidal CdSe Platelets with Thicknesses Controlled at the Atomic Level. *J. Am. Chem. Soc.* **2008**, *130*, 16504–16505.
- (10) Akkerman, Q. A.; Motti, S. G.; Srimath Kandada, A. R.; Mosconi, E.; D'Innocenzo, V.; Bertoni, G.; Marras, S.; Kamino, B. A.; Miranda, L.; De Angelis, F.; Petrozza, A.; Prato, M.; Manna, L. Solution Synthesis Approach to Colloidal Cesium Lead Halide Perovskite Nanoplatelets with Monolayer-Level Thickness Control. *J. Am. Chem. Soc.* **2016**, *138*, 1010–1016.
- (11) Tyagi, P.; Arveson, S. M.; Tisdale, W. A. Colloidal Organohalide Perovskite Nanoplatelets Exhibiting Quantum Confinement. *J. Phys. Chem. Lett.* **2015**, *6*, 1911–1916.
- (12) Weidman, M. C.; Seitz, M.; Stranks, S. D.; Tisdale, W. A. Highly Tunable Colloidal Perovskite Nanoplatelets through Variable Cation, Metal, and Halide Composition. *ACS Nano* **2016**, *10*, 7830–7839.
- (13) Bekenstein, Y.; Koscher, B. A.; Eaton, S. W.; Yang, P.; Alivisatos, A. P. Highly Luminescent Colloidal Nanoplates of Perovskite Cesium Lead Halide and Their Oriented Assemblies. *J. Am. Chem. Soc.* **2015**, *137*, 16008–16011.
- (14) Achtstein, A. W.; Schliwa, A.; Prudnikau, A.; Hardzei, M.; Artemyev, M. V.; Thomsen, C.; Woggon, U. Electronic Structure and Exciton-Phonon Interaction in Two-Dimensional Colloidal CdSe Nanosheets. *Nano Lett.* **2012**, *12*, 3151–3157.
- (15) Benchamekh, R.; Gippius, N. A.; Even, J.; Nestoklon, M. O.; Jancu, J. M.; Ithurria, S.; Dubertret, B.; Efros, A. L.; Voisin, P. Tight-Binding Calculations of Image-Charge Effects in Colloidal Nanoscale Platelets of CdSe. *Phys. Rev. B: Condens. Matter Mater. Phys.* **2014**, *89*, No. 035307.
- (16) Richter, M. Nanoplatelets as Material System between Strong Confinement and Weak Confinement. *Phys. Rev. Mater.* **2017**, *1*, No. 016001.
- (17) Rajadell, F.; Climente, J. I.; Planelles, J. Excitons in Core-Only, Core-Shell and Core-Crown CdSe Nanoplatelets: Interplay between In-Plane Electron-Hole Correlation, Spatial Confinement, and Dielectric Confinement. *Phys. Rev. B: Condens. Matter Mater. Phys.* **2017**, *96*, No. 035307.
- (18) Zhang, Y.; Mascarenhas, A. Scaling of Exciton Binding Energy and Virial Theorem in Semiconductor Quantum Wells and Wires. *Phys. Rev. B: Condens. Matter Mater. Phys.* **1999**, *59*, 2040–2044.
- (19) Naem, A.; Masia, F.; Christodoulou, S.; Moreels, I.; Borri, P.; Langbein, W. Giant Exciton Oscillator Strength and Radiatively Limited Dephasing in Two-Dimensional Platelets. *Phys. Rev. B: Condens. Matter Mater. Phys.* **2015**, *91*, No. 121302.
- (20) Scott, R.; Achtstein, A. W.; Prudnikau, A. V.; Antanovich, A.; Siebbeles, L. D. A.; Artemyev, M.; Woggon, U. Time-Resolved Stark Spectroscopy in CdSe Nanoplatelets: Exciton Binding Energy, Polarizability, and Field-Dependent Radiative Rates. *Nano Lett.* **2016**, *16*, 6576–6583.
- (21) Berkelbach, T. C.; Hybertsen, M. S.; Reichman, D. R. Theory of Neutral and Charged Excitons in Monolayer Transition Metal Dichalcogenides. *Phys. Rev. B: Condens. Matter Mater. Phys.* **2013**, *88*, No. 045318.
- (22) Ugeda, M. M.; Bradley, A. J.; Shi, S. F.; Da Jornada, F. H.; Zhang, Y.; Qiu, D. Y.; Ruan, W.; Mo, S. K.; Hussain, Z.; Shen, Z. X.; Wang, F.; Louie, S. G.; Crommie, M. F. Giant Bandgap Renormalization and Excitonic Effects in a Monolayer Transition Metal Dichalcogenide Semiconductor. *Nat. Mater.* **2014**, *13*, 1091–1095.
- (23) Tarucha, S.; Okamoto, H.; Iwasa, Y.; Miura, N. Exciton Binding Energy in GaAs Quantum Wells Deduced from Magneto-Optical Absorption Measurement. *Solid State Commun.* **1984**, *52*, 815–819.
- (24) Tran Thoai, D. B. Exciton Binding Energy in Semiconductor Quantum Wells and in Heterostructures. *Phys. B* **1990**, *164*, 295–299.
- (25) Miller, D. A. B.; Chemla, D. S.; Damen, T. C.; Gossard, A. C.; Wiegmann, W.; Wood, T. H.; Burrus, C. A. Electric Field Dependence of Optical Absorption near the Band Gap of Quantum-Well Structures. *Phys. Rev. B: Condens. Matter Mater. Phys.* **1985**, *32*, 1043–1060.
- (26) Miller, D. A. B. Optical Physics of Quantum Wells. In *Quantum Dynamics of Simple Systems*; Oppo, G. L., Barnet, S. M., Riis, E., Wilkinson, M., Eds.; CRC Press: Boca Raton, FL, 2017; pp 239–266.
- (27) Stier, A. V.; McCreary, K. M.; Jonker, B. T.; Kono, J.; Crooker, S. A. Exciton Diamagnetic Shifts and Valley Zeeman Effects in Monolayer WS<sub>2</sub> and MoS<sub>2</sub> to 65 T. *Nat. Commun.* **2016**, *7*, 10643.
- (28) Stier, A. V.; Wilson, N. P.; Clark, G.; Xu, X.; Crooker, S. A. Probing the Influence of Dielectric Environment on Excitons in Monolayer WSe<sub>2</sub>: Insight from High Magnetic Fields. *Nano Lett.* **2016**, *16*, 7054–7060.
- (29) Stier, A. V.; Wilson, N. P.; Velizhanin, K. A.; Kono, J.; Xu, X.; Crooker, S. A. Magneto-optics of Exciton Rydberg States in a Monolayer Semiconductor. *Phys. Rev. Lett.* **2018**, *120*, No. 057405.
- (30) Plechinger, G.; Nagler, P.; Arora, A.; Granados Del Águila, A.; Ballottin, M. V.; Frank, T.; Steinleitner, P.; Gmitra, M.; Fabian, J.; Christianen, P. C. M.; Bratschitsch, R.; Schüller, C.; Korn, T. Excitonic Valley Effects in Monolayer WS<sub>2</sub> under High Magnetic Fields. *Nano Lett.* **2016**, *16*, 7899–7904.
- (31) Chernikov, A.; Berkelbach, T. C.; Hill, H. M.; Rigosi, A.; Li, Y.; Aslan, O. B.; Reichman, D. R.; Hybertsen, M. S.; Heinz, T. F. Exciton Binding Energy and Nonhydrogenic Rydberg Series in Monolayer WS<sub>2</sub>. *Phys. Rev. Lett.* **2014**, *113*, No. 076802.
- (32) Nash, K. J.; Skolnick, M. S.; Claxton, P. A.; Roberts, J. S. Diamagnetism as a Probe of Exciton Localization in Quantum Wells. *Phys. Rev. B: Condens. Matter Mater. Phys.* **1989**, *39*, 10943–10954.
- (33) Walck, S. N.; Reinecke, T. L. Exciton Diamagnetic Shift in Semiconductor Nanostructures. *Phys. Rev. B: Condens. Matter Mater. Phys.* **1998**, *57*, 9088–9096.
- (34) Stier, A. V.; McCreary, K. M.; Jonker, B. T.; Kono, J.; Crooker, S. A. Magneto-Reflection Spectroscopy of Monolayer Transition-Metal Dichalcogenide Semiconductors in Pulsed Magnetic Fields. *J. Vac. Sci. Technol., B: Nanotechnol. Microelectron.: Mater., Process., Meas., Phenom.* **2016**, *34*, 04J102.
- (35) Bugajski, M.; Kuszko, W.; Reginski, K. Diamagnetic Shift of Exciton Energy Levels in GaAs-Ga<sub>1-x</sub>Al<sub>x</sub>As Quantum Wells. *Solid State Commun.* **1986**, *60*, 669–673.
- (36) Shields, P. A.; Nicholas, R. J.; Grandjean, N.; Massies, J. Magneto-Photoluminescence of AlGaIn/GaN Quantum Wells. *J. Cryst. Growth* **2001**, *230*, 487–491.
- (37) Cunningham, P. D.; Souza, J. B.; Fedin, I.; She, C.; Lee, B.; Talapin, D. V. Assessment of Anisotropic Semiconductor Nanorod and Nanoplatelet Heterostructures with Polarized Emission for Liquid Crystal Display Technology. *ACS Nano* **2016**, *10*, 5769–5781.
- (38) Beaudoin, E.; Davidson, P.; Abecassis, B.; Bizien, T.; Constantin, D. Reversible Strain Alignment and Reshuffling of Nanoplatelet Stacks Confined in a Lamellar Block Copolymer Matrix. *Nanoscale* **2017**, *9*, 17371–17377.
- (39) Gao, Y.; Weidman, M. C.; Tisdale, W. A. CdSe Nanoplatelet Films with Controlled Orientation of Their Transition Dipole Moment. *Nano Lett.* **2017**, *17*, 3837–3843.
- (40) Suarez, I.; Munoz, R.; Chirvony, V.; Martinez-Pastor, J.; Artemyev, M.; Prudnikau, A.; Antanovich, A.; Mikhailov, A. Multilayers of CdSe/CdS/ZnCdS Core/Wings/Shell Nanoplatelets Integrated in a Polymer Waveguide. *IEEE J. Sel. Top. Quantum Electron.* **2017**, *23*, 1.
- (41) Erdem, O.; Gungor, K.; Guzelurk, B.; Tanriover, I.; Sak, M.; Olutas, M.; Dede, D.; Kelestermur, Y.; Demir, H. V. Orientation-Controlled Nonradiative Energy Transfer to Colloidal Nanoplatelets: Engineering Dipole Orientation Factor. *Nano Lett.* **2019**, DOI: 10.1021/acsnanolett.9b00681.
- (42) Wang, L.-W.; Zunger, A. Electronic Structure Pseudopotential Calculations of Large (~1000 Atoms) Si Quantum Dots. *J. Phys. Chem.* **1994**, *98*, 2158–2165.
- (43) Rabani, E.; Hetényi, B.; Berne, B. J.; Brus, L. E. Electronic Properties of CdSe Nanocrystals in the Absence and Presence of a Dielectric Medium. *J. Chem. Phys.* **1999**, *110*, 5355–5369.

(44) Rohlfing, M.; Louie, S. G. Electron-Hole Excitations and Optical Spectra from First Principles. *Phys. Rev. B: Condens. Matter Mater. Phys.* **2000**, *62*, 4927–4944.

(45) Diroll, B. T.; Fedin, I.; Darancet, P.; Talapin, D. V.; Schaller, R. D. Surface-Area-Dependent Electron Transfer between Isoenergetic 2D Quantum Wells and a Molecular Acceptor. *J. Am. Chem. Soc.* **2016**, *138*, 11109–11112.

(46) Jana, S.; Phan, T. N. T.; Bouet, C.; Tessier, M. D.; Davidson, P.; Dubertret, B.; Abécassis, B. Stacking and Colloidal Stability of CdSe Nanoplatelets. *Langmuir* **2015**, *31*, 10532–10539.

(47) Beaudoin, E.; Abecassis, B.; Constantin, D.; Degrouard, J.; Davidson, P. Strain-Controlled Fluorescence Polarization in a CdSe Nanoplatelet–block Copolymer Composite. *Chem. Commun.* **2015**, *51*, 4051–4054.

(48) Matsunaga, T.; Endo, H.; Takeda, M.; Shibayama, M. Microscopic Structure Analysis of Clay-Poly(Ethylene Oxide) Mixed Solution in a Flow Field by Contrast-Variation Small-Angle Neutron Scattering. *Macromolecules* **2010**, *43*, 5075–5082.

(49) Dykes, L. M. C.; Torkelson, J. M.; Burghardt, W. R.; Krishnamoorti, R. Shear-Induced Orientation in Polymer/Clay Dispersions via *In Situ* X-Ray Scattering. *Polymer* **2010**, *51*, 4916–4927.

(50) Kunneman, L. T.; Schins, J. M.; Pedetti, S.; Heuclin, H.; Grozema, F. C.; Houtepen, A. J.; Dubertret, B.; Siebbeles, L. D. A. Nature and Decay Pathways of Photoexcited States in CdSe and CdSe/CdS Nanoplatelets. *Nano Lett.* **2014**, *14*, 7039–7045.

(51) Wall, M. R.; Neuhauser, D. Extraction, through Filter-Diagonalization, of General Quantum Eigenvalues or Classical Normal Mode Frequencies from a Small Number of Residues or a Short-Time Segment of a Signal. I. Theory and Application to a Quantum-Dynamics Model. *J. Chem. Phys.* **1995**, *102*, 8011–8022.

(52) Toledo, S.; Rabani, E. Very Large Electronic Structure Calculations Using an Out-of-Core Filter-Diagonalization Method. *J. Comput. Phys.* **2002**, *180*, 256–269.